RESEARCH ARTICLE

WILEY

Myosin's powerstroke occurs prior to the release of phosphate from the active site

Brent Scott | Christopher Marang | Mike Woodward | Edward P. Debold

Department of Kinesiology, University of Massachusetts, Amherst, Massachusetts

Correspondence
Edward P. Debold, Muscle Biophysics Lab, University of Massachusetts, Amherst, MA, 01003, USA.
Email: edebold@umass.edu

Abstract

Myosins are a family of motor proteins responsible for various forms of cellular motility, including muscle contraction and vesicular transport. The most fundamental aspect of myosin is its ability to transduce the chemical energy from the hydrolysis of ATP into mechanical work, in the form of force and/or motion. A key unanswered question of the transduction process is the timing of the force-generating powerstroke relative to the release of phosphate (P_i) from the active site. We examined the ability of single-headed myosin Va to generate a powerstroke in a single molecule laser trap assay while maintaining P_i in its active site, by either elevating P_i in solution or by introducing a mutation in myosin's active site (S217A) to slow P_i-release from the active site. Upon binding to the actin filament, WT myosin generated a powerstoke rapidly (≥ 500 s^{-1}) and without a detectable delay, both in the absence and presence of 30 mM P_i. The elevated levels of P_i did, however, affect event lifetime, eliminating the longest 25% of binding events, confirming that P_i rebound to myosin's active site and accelerated detachment. The S217A construct also generated a powerstroke similar in size and rate upon binding to actin despite the slower P_i release rate. These findings provide direct evidence that myosin Va generates a powerstroke with P_i still in its active site. Therefore, the findings are most consistent with a model in which the powerstroke occurs prior to the release of P_i from the active site.

KEYWORDS
force-generation, myosin, phosphate-release, powerstroke

1 | INTRODUCTION

Myosins are a family of motor proteins responsible for generating force and/or motion inside the cell (Foth, Goedecke, & Soldati, 2006). Muscle myosin II is the most well-characterized class and is the molecular motor that drives muscle contraction (Geeves & Holmes, 1999). Myosin Va has a motor domain that is highly homologous to myosin II (Foth et al., 2006) but its task is the intracellular transport of vesicles, walking processively along the 36 nm pseudo-repeat of actin filaments (Warshaw et al., 2005; Yildiz et al., 2003). Other forms of

myosin and related molecular motors (e.g., kinesin) play important roles in intracellular transport, cell migration, the maintenance of cell structure, and even in mitosis (Foth et al., 2006).

Common to all myosins is the ability to convert the chemical energy of ATP into mechanical work, however key molecular details of this process remain unclear (Houdusse & Sweeney, 2016; Takagi, Homsher, Goldman, & Shuman, 2006). In a precisely coordinated sequence of steps the ATP is hydrolyzed off of actin and then the products are released while it is tightly bound to an actin filament (Holmes & Geeves, 2000; Sweeney & Houdusse, 2010). In a simple model of the cross-bridge cycle, ATP enters the active site with myosin tightly bound to actin in the apo or rigor state. This induces

conformational changes that cause myosin to dissociate from actin (Geeves & Holmes, 2005). ATP is then hydrolyzed to ADP and P_i off of actin, but the products remain in the active site while myosin is detached from actin. The re-binding to actin triggers the release of P_i and then ADP (Bagshaw & Trentham, 1974). The powerstroke is thought to occur close in time to the release of P_i (Holmes & Geeves, 2000; Houdusse & Sweeney, 2016; Sweeney & Houdusse, 2010; Takagi, Shuman, & Goldman, 2004) from the active site, however the exact sequence of events is unclear and is currently the source of a vigorous debate within the field (Gunther et al., 2020; Llinas et al., 2015; Muretta, Rohde, Johnsrud, Cornea, & Thomas, 2015; Trivedi et al., 2015; Woody, Winkelmann, Capitanio, Ostap, & Goldman, 2019). The key unanswered question is which event occurs first the powerstroke or the release of P_i from the active site (Llinas et al., 2015; Woody et al., 2019)? In other words, does the mechanical event "gate" the biochemical changes, or do the chemical reactions "gate" the mechanical events? The answer to this question has important implications for the long-standing pursuit of the molecular basis of force-generation by muscle (Huxley & Simmons, 1971; Linari et al., 2015; Piazzesi et al., 2002; Veigel, Molloy, Schmitz, & Kendrick-Jones, 2003), but it also has broader implications for understanding the fundamental nature of energy transduction by nucleotide-based motor proteins (Vale, 1996, 2003).

The timing of force-generation relative to P_i-release was first addressed in single skeletal muscle fibers (myosin II); these studies demonstrated that the development of force preceded the release of the first hydrolysis product, P_i (He et al., 1997; Sleep, Irving, & Burton, 2005). Consistent with these observations, the rapid release of caged-P_i demonstrated a clear delay in the depression of isometric force in muscle fibers (Dantzig, Goldman, Millar, Lacktis, & Homsher, 1992). These findings were consistent with force-generation preceding the release of P_i; however, the spatial and temporal resolution of these assays could not provide direct evidence of how and when a single myosin was progressing through its mechanical or biochemical transitions. More molecular level detail was provided by work using Förster Resonance Energy Transfer (FRET) probes on isolated myosin molecules in bulk solution assays, to directly monitor the position of the lever arm while also tracking the rate of P_i-release using a rapid-reporting, phosphate-binding-protein (Muretta et al., 2015; Trivedi et al., 2015). These assays demonstrated that lever arm rotation occurred rapidly after myosin strongly bound to actin, at a rate of $\geq 350 \cdot s^{-1}$, while P_i-release from the strongly bound state occurred at $\sim 30 \cdot s^{-1}$, suggesting that P_i-release occurs after lever arm rotation for myosin II. Similar findings were observed using myosin Va with the powerstroke occurring at $400 \cdot s^{-1}$, while P_i-release occurred at $200 \cdot s^{-1}$ (Trivedi et al., 2015). Similarly, single molecule observations, with microsecond time resolution, suggest that in cardiac myosin lever arm rotation may occur even faster, at $1000-5000 \cdot s^{-1}$ (Woody et al., 2019), exceeding all estimates of P_i-release from myosin II by at least an order of magnitude (Sleep et al., 2005). Thus, the findings from these types of functional assays support the hypothesis that the powerstroke occurs prior to P_i-release.

However, x-ray crystallography structures of myosin, captured in various states of the cross-bridge cycle, suggest that P_i-release must occur before lever arm rotation (Llinas et al., 2015; Sweeney & Houdusse, 2010). Specifically, structures of myosin trapped in different nucleotide states using various nucleotide analogs show that the lever arm exists in a pre-powerstroke position when the gamma-P_i (or an equivalent analog) is still in the active site, and only achieves a post-powerstoke position when the gamma-P_i is absent from the active site (Robert-Paganin et al., 2020). Based on these and similar structural observations it was hypothesized that upon binding to actin, conformational changes in myosin's active site occur that allow P_i to be released from the active site, and only then can the conformational changes that lead to lever arm rotation occur. Thus, this hypothesis posits that P_i-release "gates" the lever arm rotation, therefore the lever arm cannot rotate (i.e., the powerstroke cannot occur) until P_i has left the active site (Gulick et al., 2000; Rayment et al., 1993a).

In attempt to resolve the conflict between the functional and structural evidence, Llinas et al. (Llinas et al., 2015) formed myosin crystals soaked in elevated levels of P_i for varying durations before rapidly freezing the samples and performing x-ray crystallography. With a short exposure time before freezing, P_i was observed to be either at the exit of the escape tunnel adjacent to the active site (P_iR1) or close to ADP in the nucleotide binding region (P_iR2, that is, still in the active site). Longer delays before freezing revealed that P_i diffused back into the active site close to ADP, and when it did, the lever arm returned to the prepowerstroke position. These observations led the authors to hypothesize that P_i leaves the active site very rapidly (and prior to the powerstroke) but stays in the exit tunnel before it is released into solution. Thus P_i-release from the active site may occur much more rapidly than P_i appears in solution. This idea could therefore potentially explain why functional assays observe a rate of P_i-release that is slower than the rate of force development and the powerstroke (Muretta et al., 2015; Trivedi et al., 2015). To further test this hypothesis, Llinas et al. (Llinas et al., 2015) introduced a mutation into switch I that was designed to slow P_i-release; by impeding it from entering the exit tunnel (S217A in myosin Va). The loss of the hydroxyl group, thought to make contact with the gamma-phosphate of ATP (Forgacs et al., 2009; Smith & Rayment, 1996), is hypothesized to impede the entry of P_i into the exit tunnel (Llinas et al., 2015). Consistent with this hypothesis, actin-activated P_i-release is 3–10-fold slower in this mutation compared to WT (Forgacs et al., 2009; Gunther et al., 2020; Llinas et al., 2015). In addition, x-ray crystal structures of myosin soaked in high concentrations of P_i for 45 min show P_i in the active site near ADP with myosin occupying a prepowerstroke state, supporting a P_i-release gated powerstroke (Llinas et al., 2015). Thus, the release of P_i may occur faster than the lever arm rotation, but it may not appear in solution immediately because it is still in the P_i exit tunnel. If correct, this would provide an explanation for the discrepancy in the results between structural and functional findings. Indeed, it was recently proposed that this structural information provides a hypothesis that unifies prior findings from solution and functional experiments (Robert-Paganin et al., 2020).

This hypothesis is also important because it makes specific and testable predications about how a single myosin molecule should behave if P_i is maintained in its active site. For example, because P_i gates the powerstroke in this model, P_i should only rebind to actomyosin in a prepowerstroke state because P_i can only leave or re-enter the active site when the lever arm is in a prepowerstroke position (Llinas et al., 2015; Sweeney & Houdusse, 2010). Indeed, in this model, the rebinding of P_i to the active site prevents the powerstroke from occurring rather than reversing it. By exposing myosin to elevated levels of P_i to maintain P_i in the active site, lever arm rotation (i.e., powerstroke) generated by myosin after it binds to actin should be delayed or even prevented if P_i gates the powerstroke. Similarly, a myosin construct with a mutation that slows the entry of P_i into the P_i exit tunnel (e.g., S217A; Forgacs et al., 2009; Llinas et al., 2015), should also dramatically delay, or even prevent, myosin from generating a powerstroke once it strongly binds to actin. These effects would be most evident at the single molecule level where the generation of a powerstroke can be directly observed, and the duration of single actomyosin interactions directly quantified. Therefore, we directly tested this hypothesis using both approaches (high levels of P_i and the S217A mutation) in a single molecule laser trap assay using a single-headed construct of myosin Va.

2 | RESULTS

To determine the order of the powerstroke relative to P_i-release from myosin's active site, we directly observed the powertroke and strongly bound lifetime of a single-headed 1IQ construct of myosin Va using a three-bead single molecule laser trap assay (Figure 1a,b). In the first series of experiments, we examined the effect of 30 mM P_i on the size of myosin's powerstroke. To ensure that the elevated P_i would preferentially rebind to an actomyosin state with ADP still in the active site (AM.ADP), the ATP concentration was maintained at 100 μM for this set of experiments, a value well above the estimated k_m of 17 μM (Baker et al., 2004; Forgacs et al., 2009). Single actomyosin interactions (Figure 1c) were detected using an algorithm based on a Hidden–Markov Model (Smith et al., 2001), and transitions into and out of single binding events were located using a Changepoint-analysis technique (Blackwell et al., 2021; see Section 5).

The 1 IQ construct of myosin Va generated a 7 ± 0.6 nm (Mean ± SEM) powerstroke (Figure 1b) that was unchanged by elevating P_i to 30 mM in the experimental solution (Figure 1e). The S217A construct also generated a step that was not statistically different from the WT myosin construct, either in the absence or presence of 30 mM P_i (Figure 1e). This suggests that when P_i-release is slowed from the active site, by either the S217A mutation (Figure 1b) or by P_i rebinding to the open active site, myosin generates the same size powerstroke upon binding to the actin filament.

To further address the relative timing of powerstroke and P_i-release, we examined the rate of the transition from the unbound/weakly bound state into the strongly bound state (Figure 2a) using an ensemble averaging analysis previously described (Sellers &

Veigel, 2010; Veigel et al., 2003), with minor modifications. In this analysis, the start and end of identified actomyosin binding events were temporally aligned (see Section 5). The front ends of the binding events were fit to a double exponential ($y = d_1*(1 - \exp[x^* - k_0]) + d_2*(1 - \exp[x^* - k_1])$) to estimate the transition rate (k_0) from the detached/weakly attached states to the postpowerstroke state, of the primary powerstroke (Figure 2a) and a second rate (k_1) reflecting the transition associated with the secondary powerstroke (see Section 5 for additional details). The initial rate, k_0, was rapid and similar in the absence and presence of P_i for both constructs (604 and 467·s^{-1} for WT at 0 and 30 mM P_i, and 597 and 757·s^{-1} for S217A at 0 and 30 mM P_i, respectively). This rate (k_0) is thought to reflect several processes including the initial Brownian capture of the actin filament by myosin and the powerstroke (Blackwell et al., 2021; Veigel et al., 2003). Furthermore, the motion of the beads is damped by the viscous forces acting on the optically trapped 1-μm diameter bead, with a corner frequency of ~500 Hz, which limits this rate (Neuman & Block, 2004). Despite these temporal constraints, if P_i-release occurred prior to the powerstroke, 30 mM P_i should have reduced this rate dramatically. This was not observed (Figure 2a).

To further investigate whether a pause occurred prior to the powerstroke, we examined the slope of the first 2 ms of the initial transitions in the ensemble averaged data (Figure 2e). During the first 2 ms of this transition, the powerstroke of myosin generates an average force of 4pN (Finer, Simmons, & Spudich, 1994), enabling it to move the damped bead more quickly than 500·s^{-1} through solution, thus making it an even more sensitive measure for detecting a delay prior to the powerstroke. 2 ms was chosen because 90% of the powerstroke was completed within this time frame and a longer time window would include the plateau after the powerstroke was completed and thus would not reflect the time during the primary powerstroke (Figure 2). The slope of linear fits to these data show that for both constructs (WT and S217A), and conditions (0 and 30 mM P_i), the transition during the first 2 ms was extremely rapid and occurred immediately upon strongly binding to the actin filament (Figure 2e). This result strongly suggests that myosin generates the powerstroke immediately upon strongly binding to the actin filament and without a delay to allow for the release of P_i from the active site.

To confirm that our analyses could detect a delay in the generation of the powerstroke if it occurred, we performed simulations of single binding events in which myosin bound to actin and either, rapidly generated a powerstroke (Figure 2b) or paused with a time constant of 30 ms before generating a step (Figure 2c). The time constant for P_i-release was chosen to be consistent with the average measured rate of P_i-release from the S217A construct from three different reports (Forgacs et al., 2009; Gunther et al., 2020; Llinas et al., 2015). Analysis of these simulated data confirmed that such a pause would have appeared as a zero slope during the first 2 ms of the binding event (Figure 2f) and would have been visible as a slowed rate of transition into the strongly bound state in the ensemble average analysis (Figure 2d). In contrast to this prediction for a P_i-release first model, we observed a very rapid transition from bound to unbound in the experimental data in both constructs, as well as in the absence and
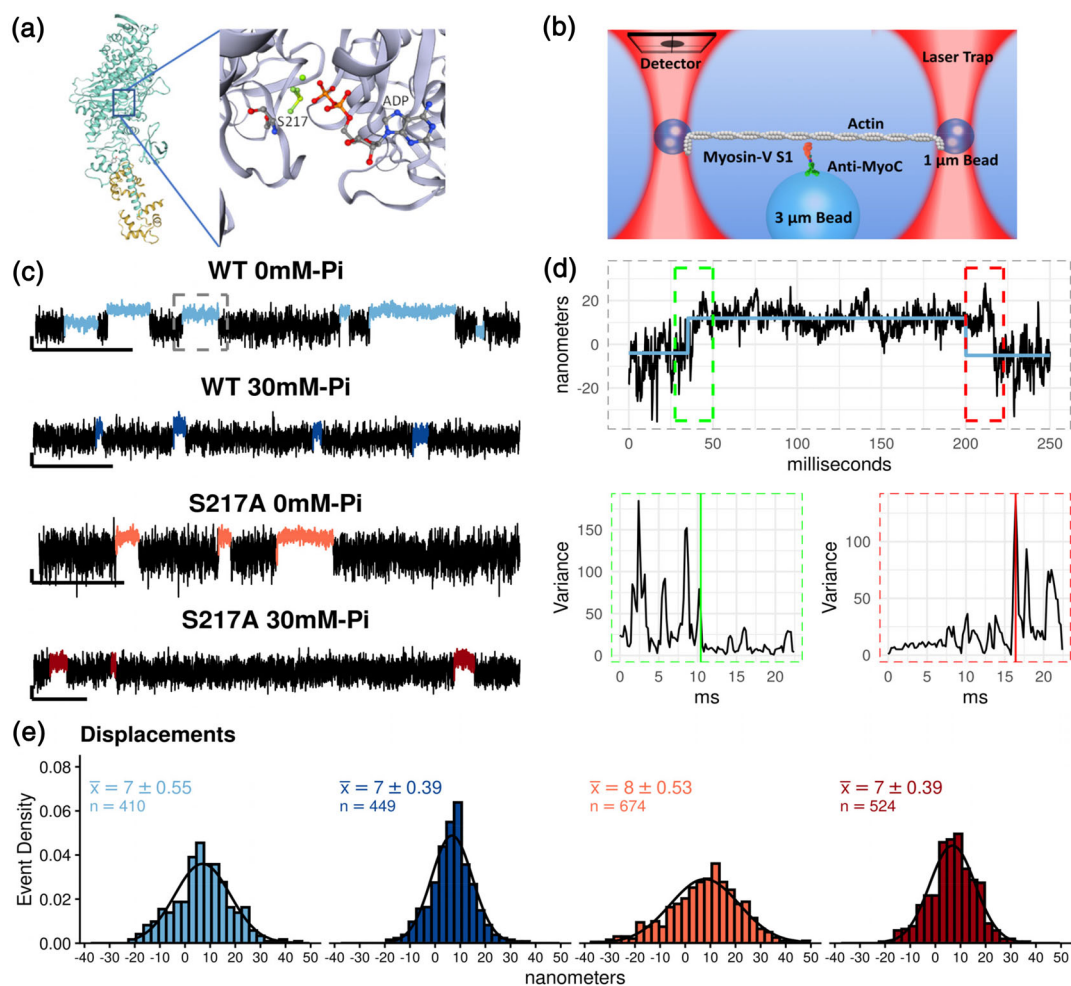
FIGURE 1 Single molecule laser trap assay data and analysis. (a) The x-ray crystal structure of myosin Va (Shen et al., 2016), left, with the heavy chain colored in teal and the single calmodulin in gold. An expanded view of the active site, right, showing the location of the S217 near the nucleotide binding site. Images rendered in Swiss PDF viewer. The expanded view of the active site is from a structure complexed with ADP-beryllium-fluoride (Coureux et al., 2004). (b) A schematic representation of the three-bead laser trap assays used. Myosin Va S1 with a single light-chain binding domain was adhered to the pedestal (3 μm bead) via an anti-myoC antibody. Displacements of the actin filament upon myosin binding were tracked using a quadrant-photodiode (detector). (c) Raw displacement traces for each myosin construct collected at 100 μM ATP, and in the presence or absence of 30 mM P_i. Scale bar indicates 20 nm in the vertical axis and 500 ms in the horizontal axis. Actomyosin strong-binding events as identified by the analysis are colored differently than baseline noise for each condition and used consistently through the text. (d) Method of event detection shown for a binding event for WT myosin at 0 mM P_i. A single binding event in "c" (dashed gray box) is used to illustrate event detection. A Hidden–Markov Model was used to identify the approximate location of a binding event (blue line in upper graph) and Change-point analysis was used to precisely determine the start, and end, of the each event (dashed green and red boxes, upper graph) based on abrupt changes in the running variance of the signal both at the start and end of the binding event (lower graphs). See Section 5 for further details of binding event detection. (e) Histogram of binding events fit to Gaussian curves. The mean ± SEM are shown with the sample size (n) indicated for both conditions and constructs. A 2-way ANOVA (myosin × P_i) analysis reported no significant ($p < .05$) differences [Color figure can be viewed at wileyonlinelibrary.com]

presence of added P_i (Figure 2e). There was also no significant effect on the rates of transitions in the ensemble average analysis in the experimental data (Figure 2d vs. a). Collectively, these findings suggest that neither elevated P_i nor the S217A substitution slowed the rate of myosin's powerstroke, or induced a pause prior to generation of the powerstroke.

While the elevated P_i did not affect the size of myosin's powerstroke in either construct, we also examined the duration of binding events for evidence that P_i rebound to myosin's active site.

Indeed, in the WT construct, elevated P_i reduced the average lifetime (Figure 3a,b) suggesting that P_i rebound to actomyosin and accelerated myosin's detachment from actin. The difference in the arithmetic means was not significant, but the mean in the WT 0 mM-P_i condition was quite far from the median, indicating a skew in the distribution (Figure 3b). Indeed, this was because the decreased lifetime was not uniform across the distribution of binding event durations, rather it was due to a reduction in the number of long duration binding events, especially those >400 ms. For example, in the presence of P_i only, one
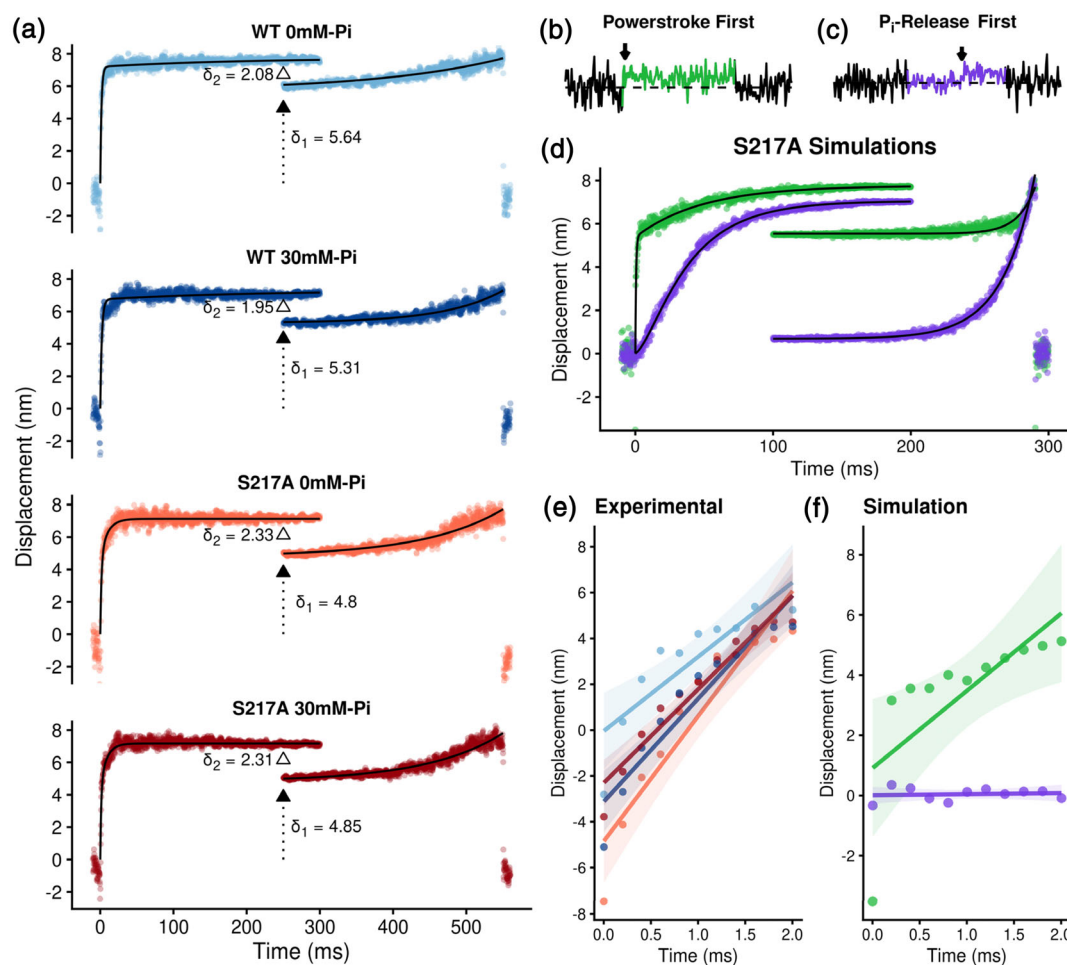
FIGURE 2 Ensemble averaged binding events. (a) Events detected as indicated in Figure 1 were aligned and averaged for each condition and construct. Both the start and end of events were temporally aligned and the start fit with a double exponential fit: $y = d_1*(1 - \exp[-k_0 * x]) + d_2*(1 - \exp[-k_1 * x])$, where d_1 is the displacement associated with the primary powerstroke and d_2 the secondary powerstroke. k_0 and k_1 represent the rates of the transition from unbound to the postpowerstoke state and the transition to the secondary powerstroke state, respectively (see Section 5). Backward ensembles were fit with single exponentials of the form: $y = d_1 + (d_2*\exp[k_2 * x])$ (see Section 5). The first component of the fit to the start of the event reflects the transition from weak/unattached to a strongly bound postpowerstroke state. These rates were 614 and 467·s^{-1} for WT myosin Va in the absence and presence of 30 mM P_i, respectively and 596 and 757·s^{-1} for the S217A construct in the absence and presence of P_i, respectively. To determine the size of the secondary powerstroke (δ_2) the average of the last 100 data points of the front end of the ensemble averaged events were subtracted from the first 100 data points of the events aligned to the back end of the events (hollow triangle). This value was then subtracted from the total displacement to determine δ_1 (filled triangle with dotted line) using methods previously described (Capitanio et al., 2006). Under both conditions (0 and 30 mM P_i) and in both constructs (WT and S217A) δ_1 and δ_2 were not significantly different. (b) Simulated single molecule binding events using either a powerstroke-first model (green) or a P_i-release-first model (purple, c). Black arrows in b and c indicate the location of the powerstroke. Details of the simulations are provided in Figure S1 of the Supplementary Materials. The red arrow indicates when the powerstroke occurs during the binding event. (d) 500 binding events were simulated for each model and then ensemble averaged using the same procedure as the experimental data (see Section 5 for details). The P_i-release first data revealed a slower rate of transition into a binding event (104 vs. 1800·s^{-1} for the P_i-release- and powerstroke-first model, respectively). (e) An expanded view of the first 2 ms of the ensemble averages. The first 2 ms were used as the transition from unbound/weakly bound prepowerstroke to strongly bound postpowerstroke is >90% complete in this time frame. Data points were fit to a least-squares linear fit, with the shaded area representing a 95% C.I. for each line fit. Additional parameters of this analysis are displayed in Table S1. (f) Ensemble averaged data from simulations of S217A data using a powerstroke-first model (green) and a P_i-release-first model (purple) [Color figure can be viewed at wileyonlinelibrary.com]

binding event lasted longer than 1,000 ms (Figure 3b). In contrast, in the absence of P_i, 25% of the events lasted longer than 500 ms (Figure 3a, main graph). The effect of P_i was most evident in a quantile-quantile (Q-Q) plot of binding event durations versus the theoretical exponential fit (Figure 3c). And a Kolmogorov–Smirnov test

revealed that there was a trend ($p = 0.06$) toward a difference between the distribution for the absence versus presence of 30 mM P_i. This finding suggests that P_i rebound to longer duration events in an AM.ADP state and accelerated detachment from actin. Elevated levels of P_i did not affect the event lifetimes of S217A, however in
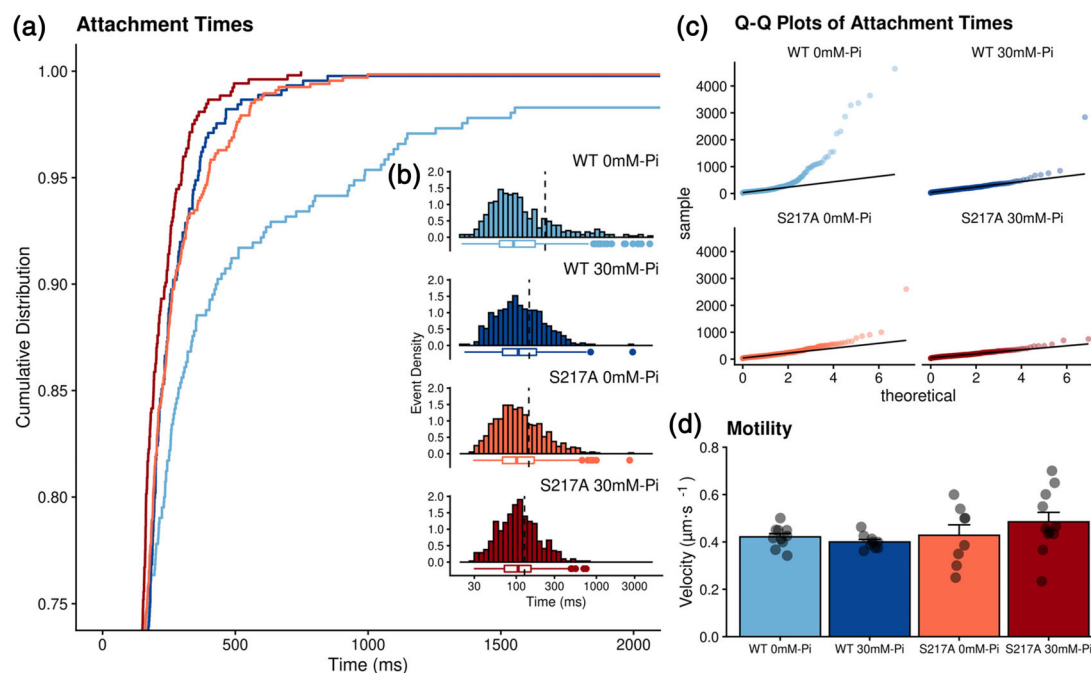
FIGURE 3 Binding event durations and bulk assays measurements. (a) Cumulative distribution of the lifetime of the single molecule binding events. Color scheme same as in Figure 1. The y-axis is truncated below 70% of events to demonstrate the effect of P_i on lifetimes. (b) inset graph, histogram of the lifetime of all binding events for each condition (P_i) and each myosin construct. Dashed vertical line indicates the arithmetic mean and boxplot underneath displays outliers >1.5 times the interquartile range. A Kruskal–Wallis, nonparametric, ANOVA was used to test for significant ($p < .05$) differences among conditions, none were observed, however the distribution of events was altered (see Section 2). (c) A quantile-quantile (Q-Q) plot showing the location and magnitude of deviation of individual event durations (points) from a theoretical single exponential fit (solid black line). A comparison of the 0 versus 30 mM P_i distributions using a Kolmogorov–Smirnov, nonparametric test reveal a trend ($p = .06$) toward a difference. (d) Bar graph of Actin filament velocities from an in vitro motility assay performed for each condition and construct. Bar represents mean ± SEM from eight experiments for each condition (points). Each data point represents the average velocity of three separate fields of view, that contained ~5–25 actin filament trajectories. Data were collected at 10 frames per second and the displacements were quantified frame by frame using MTrackJ (ImageJ plugin) as previously described (Debold, Turner, Stout, & Walcott, 2011). Data collected at 2 mM ATP at 125 mM total ionic strength. No significant ($p < .05$) differences were detected with a one-way ANOVA [Color figure can be viewed at wileyonlinelibrary.com]

absence of P_i this construct has a shorter bound lifetime than the WT (Figure 3a,b), which likely reflects acceleration in the ADP-release rate caused by this substitution (Forgacs et al., 2009; Gunther et al., 2020). The accelerated rate of ADP-release may reduce its vulnerability to the rebinding of P_i, providing an explanation for the absence of a P_i-induced reduction in binding event durations (Figure 3b).

The frequency of binding events was determined by dividing the total number of binding events by the total amount of time collected. The values were 0.99 and $0.98 \cdot s^{-1}$ for WT myosin Va in the absence and presence of 30 mM P_i, respectively; and 0.99 and $1.00 \cdot s^{-1}$ for the S217A construct in the absence and presence of 30 mM P_i, respectively. These findings are consistent with myosin's attachment rate being unaffected by elevated P_i or by the presence of the S217A mutation.

To determine the fate of the cross-bridge following the powerstroke and the rebinding of P_i, we again used the ensemble averaging analysis. A similar analysis has been used previously to detect and quantify the putative secondary powerstroke, or hitch, that is temporally associated with ADP-release by myosin (Sellers & Veigel, 2010; Veigel et al., 2003). We determined the size of the hitch

by quantifying the difference in magnitude between the final displacements found at the ends of the forward ensembles and the displacement found at the beginning of the backwards ensembles, for each condition (Figure 2a). This analysis confirmed that WT myosin Va generates a hitch that was 25% of the total displacement (~2 nm) consistent with previous estimates using a myosin Va construct with a longer lever arm (Sellers & Veigel, 2010). Elevated levels of P_i did not affect the magnitude of the hitch, nor did the presence of the S217A mutation (Figure 2a). However, given that only the longest 25% of binding events were affected by P_i (Figure 3a,b) it is possible that the rebinding of P_i did occur prior to the hitch. This was also likely due to the limited amount of time spent in rigor at the final posthitch displacement at the relatively high 100 μM [ATP], a concentration needed to ensure that P_i primarily rebound to the AM.ADP state.

Previous reports suggest that the rebinding of P_i to actomyosin in the AM.ADP state can induce the reversal of the powerstroke, especially when the cross-bridge is strained (Woody et al., 2019). In our assay this would have appeared as displacement in the opposite direction to the initial powerstroke, which would have occurred sometime after the initial powerstroke but while myosin remained strongly

bound to the actin filament. However, we did not see any evidence of this behavior either in the raw displacement records (Figure 1c), or in the ensemble average analysis (Figure 3a), where a reversal should have appeared as a downward slope in the transition out of a binding event, as others have observed (Woody et al., 2019).

It is possible that any reversal of the powerstroke and subsequent detachment from actin occurred faster than the resolution of our instrumentation (~2 ms). Therefore, we measured the effect of 30 mM P_i on the velocity of actin filaments in an in vitro motility assay (V_{actin}, Figure 3d); if P_i induced a reversal of the powerstroke we would expect that V_{actin} would be decreased by the presence of P_i in this assay. However, V_{actin} was unaffected by 30 mM P_i concentration (Figure 3c). Thus, under the present conditions, the rebinding of P_i does not appear to cause a reversal of the powerstroke in an S1 construct of myosin Va, despite accelerating the detachment rate in WT of the longest 25% of events (Figure 3a).

3 | DISCUSSION

3.1 | The powerstroke precedes P_i-release from the active site

Functional evidence from both myosin II and myosin V suggests that the powerstroke occurs prior to P_i-release (Muretta et al., 2015; Sleep et al., 2005; Trivedi et al., 2015; Woody et al., 2019), while recent structural evidence from x-ray crystallography studies led to the notion that P_i-release must occur prior to the powerstroke (Houdusse & Sweeney, 2016; Llinas et al., 2015; Robert-Paganin et al., 2020). Based on new structural insights, it was proposed (Llinas et al., 2015) that this seemingly contradictory evidence could be resolved if P_i is released from the active site very rapidly but pauses temporarily in the P_i exit tunnel, before being released into solution. Structural evidence was provided to support this model, including the use of the S217A mutation in switch I which slows P_i-release from the active site (Forgacs et al., 2009; Llinas et al., 2015).

We directly tested this new model in two ways; first, by elevating P_i, and second by introducing a mutation that slows P_i-release from the active site. Using the WT construct, we found that in the presence of 30 mM P_i myosin generated a powerstroke that was similar in size (Figure 1e) and rate (Figure 2e) to that observed in the absence of P_i. In this experiment, the elevated P_i in the buffer enables P_i to rebind to the active site, therefore if P_i-release gates the powerstroke, the P_i would rebind to myosin prior to the generation of a powerstroke. This would have been evident at the single molecule level as a reduction in the size and rate of the powerstroke. However, no reductions in the size or the rate of the powerstroke were observed (Figures 1 and 2). Additionally, the altered distribution of strongly bound lifetimes (Figure 3a–c) provides evidence that P_i rebinds to myosin's active site, because P_i is known to decrease myosin's affinity for actin, thereby accelerating detachment (Geeves & Holmes, 2005; Holmes & Geeves, 2000; Takagi et al., 2004). Thus, the most likely scenario in this experiment (see blue arrows in Figure 4) is that myosin initially

bound to the actin filament, and rapidly generated a powerstroke ($\geq 500 \cdot s^{-1}$, see Figure 2a,e) that was similar in size to that observed in the absence of P_i (Figure 1e). Myosin then released P_i, at a rate of 150–200$\cdot s^{-1}$(Cruz, Wells, Rosenfeld, Ostap, & Sweeney, 1999; Forgacs et al., 2009; Llinas et al., 2015; Rosenfeld & Sweeney, 2004; Trivedi et al., 2015), but in 25% of the events a new P_i from solution quickly rebound in the active site while myosin was in an AM.ADP state. The rebinding of P_i then induced detachment from actin leading to a detached M.ADP.P_i state, which produced an alteration in event lifetimes (Figure 3a–c).

This scenario suggests that the rebinding of P_i induces detachment by inducing the opening of the cleft in the upper 50 kDa domain, which modulates myosin's affinity for actin and is putatively coupled to the presence of P_i in the active site (Geeves & Holmes, 2005). Interestingly, this suggests that there might be hysteresis in the transduction process, as myosin appears to be able to bind strongly to actin with P_i still in the active site during force-generation, but rapidly detaches from actin upon P_i-rebinding. We (Debold et al., 2013) and others (Linari, Caremani, & Lombardi, 2010) have suggested a model for this hysteresis based on observations in skeletal muscle myosin II.

In a second test of the P_i-release-first model, we used a myosin Va S1 construct with S217A mutation in the switch I region of the active site, which has been shown to slow P_i-release from the active site by ~10-fold (Forgacs et al., 2009; Gunther et al., 2020; Llinas et al., 2015). Serine 217 (myosin Va numbering) is an absolutely conserved residue that is the first serine in the NDNSSRFG sequence of switch I (Forgacs et al., 2009). Its OH-group putatively forms hydrogen bonds with the gamma-phosphate, ATP and the NH_2 of Arginine 215, and it is thought to participate in proton transfer during the hydrolysis process (Forgacs et al., 2009; Smith & Rayment, 1996). The S217A mutation removes the ability of the OH-group to participate in proton transfer and likely weakens the contacts between switch-I and the gamma-phosphate of ATP (Forgacs et al., 2009).

This mutation also appears to slow the weak- to strong-binding transition, based on observations from solution kinetics; an effect that likely also contributes to the reduced steady-state ATPase rate (Forgacs et al., 2009; Gunther et al., 2020). However, the most relevant effect for the present study is the 10-fold reduction in the release of P_i from actomyosin (Forgacs et al., 2009), which occurs by slowing its release from the active site (Llinas et al., 2015). Importantly, the slowed rate of P_i-release from this construct means it is not reliant on P_i rebinding to the active site as in the experiments with elevated P_i in solution. This provides an independent test of the hypothesis that P_i-release from the active site gates myosin's powerstroke. The predicted outcome in the laser trap assay, however, is the same if P_i-release precedes the powerstroke. Myosin should bind to actin, and only after a long delay that allows for P_i to be released from the active site, should it generate a powerstroke. Contrary to this prediction, we observed that the S217A construct did not affect the size (Figure 1e) or rate (Figure 2e) of the powerstroke generated, consistent with our cursory examination of this construct using a less sophisticated analysis (Gunther et al., 2020). Our
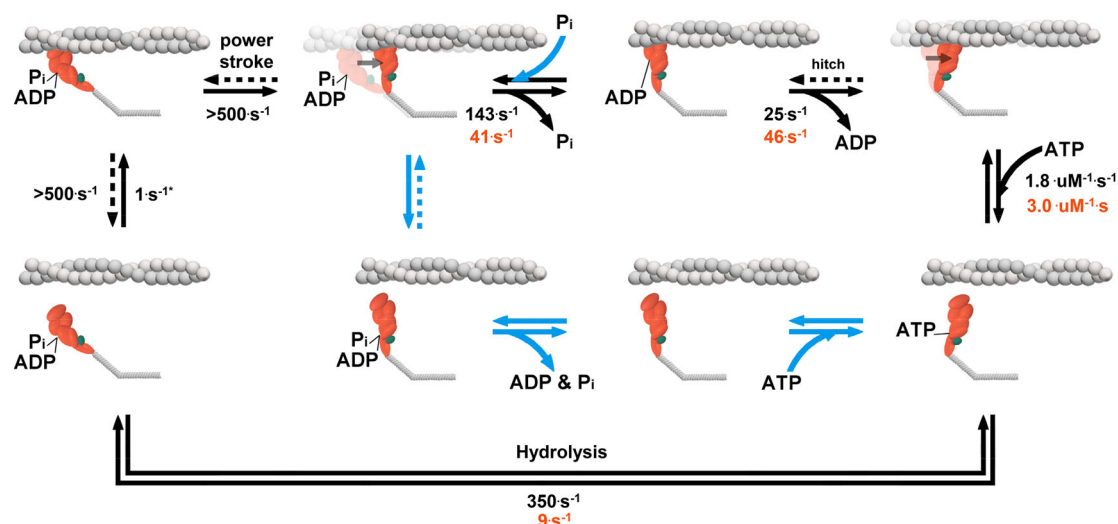
FIGURE 4 Proposed model of cross-bridge cycle. A simplified model postulating the effects of P_i and the S217A myosin's cross-cycle. The pathway followed by wild-type is shown with black arrows and numbers, with the P_i-dependent changes shown with blue arrows. The rates for the S217A are only displayed where they differed from WT myosin (orange numbers). Progressing from left to right, the attachment rate ($1\ s^{-1}$ *) is taken from the frequency binding events (see Section 2). We did not observe a distinct population of events generating zero displacement (Figure 1e) suggesting that the rate of detachment from a prepowerstroke state, if it occurs, is faster than the time resolution of our event detection (~2 ms). The key finding is that for both constructs, and in the absence of presence of 30 mM P_i the powerstroke occurred immediately upon binding to actin, consistent with work from myosin II in an ultra-fast laser trap assay at $1000 \cdot s^{-1}$ (Capitanio et al., 2012; Woody et al., 2019). No evidence was observed of a reversal of the hitch (dashed line). The P_i-release rate for WT and S217A represent the maximum actin activated rate from (Llinas et al., 2015). Since P_i reduced the bound lifetime (Figure 3a) we believe that P_i rebinds to an AM.ADP state and induces detachment from a postpowerstroke state (Debold, Walcott, Woodward, & Turner, 2013). Elevated P_i only eliminated the longest 25% of binding events in the WT myosin and not S217A (Figure 3a), thus this pathway was not active in the S217A under the present conditions. We also did not see evidence that P_i reduced the step size, suggesting that myosin in the ADP.P_i state did not readily reattach to actin in the post powerstroke state after P_i induced detachment (dashed blue line). The ADP-release rate and the secondary powerstroke (i.e., hitch) were combined for simplicity, but may occur in distinct steps (Gunther et al., 2020). Values for ATP-binding and hydrolysis are taken from estimates in solution (Forgacs et al., 2009; Gunther et al., 2020). Hydrolysis and the recovery stroke were combined for simplicity but likely occur at different rates (Gunther et al., 2020) [Color figure can be viewed at wileyonlinelibrary.com]

simulations of a P_i-release-first model confirmed that our analysis of these data had the sensitivity to detect a change in either variable (Figure 2b,c). This, like the observation with WT myosin in the presence of P_i, suggests that upon strongly binding to actin, myosin rapidly generates a powerstroke with P_i still in its active site.

These findings and conclusions are consistent with previous FRET-based studies showing that the powerstroke occurs at least twice as fast as P_i-release into solution (Muretta et al., 2015; Trivedi et al., 2015). However, the use of the S217A construct in the present investigation demonstrates that the powerstroke occurs while P_i is still in myosin's active site. Therefore, these findings would be inconsistent with a model in which P_i is released quickly from the active site before stalling the exit tunnel (Houdusse & Sweeney, 2016; Robert-Paganin et al., 2020; Sweeney & Houdusse, 2010) because this mutation prevents entry into the exit tunnel (Llinas et al., 2015). Our conclusion is also consistent with recent findings from cardiac muscle myosin using an ultra-fast laser trap assay where the rate of the powerstroke was estimated to be $1,000 \cdot s^{-1}$ under a 1.5pN resistive load (Woody et al., 2019), roughly 50-fold faster than P_i-release for cardiac myosin (Gunther et al., 2019; Malik et al., 2011). Similar rates of the powerstoke were reported in the first description of an ultra-

fast laser trap assay using fast skeletal muscle myosin II under a 1.5 pN resistive load (Capitanio et al., 2012), a rate 2 orders of magnitude faster than the $20–30 \cdot s^{-1}$ rate of P_i-release in solution reported for fast skeletal myosin II (Muretta et al., 2015). Interestingly, the rate of the powerstroke has been shown to increase with the applied resistive load (Capitanio et al., 2012; Woody et al., 2019) therefore the rate observed in the present study ($\geq 500 \cdot s^{-1}$) under the minimal load of our laser trap assay (7 nm $\times$ 0.04 pN/nm $\approx$ 0.28pN) appears consistent with the $1000–5000 \cdot s^{-1}$ rate from 1.5 to 5 pN of resistive load in an ultra-fast laser trap assay using skeletal and cardiac myosin II (Capitanio et al., 2012; Woody et al., 2019).As indicated above the present findings are difficult to reconcile with the idea that P_i-release precedes the powerstroke, as has been suggested based on high resolution crystal structures (Houdusse & Sweeney, 2016; Robert-Paganin et al., 2020; Sweeney & Houdusse, 2010). Indeed, for our data to be consistent with a P_i-release-first model, P_i would have to be released from the active site at $>1000 \cdot s^{-1}$, and then remain in the exit tunnel until it appeared in solution at a rate of $\sim 150 \cdot s^{-1}$ for the WT myosin Va construct. P_i would have to remain in the exit tunnel for an even longer duration in the S217A construct, where the rate of P_i-release rate is reduced to $15–20 \cdot s^{-1}$(Forgacs et al., 2009). Indeed, P_i would

need to be released from the active site at $>1000 \cdot s^{-1}$, but remain in the exit tunnel for roughly 50 ms, before it is released into solution, at the rate measured for the S217A construct $15–20 \cdot s^{-1}$. This seems an inordinately long duration for P_i to remain trapped in the exit tunnel given that the putative contacts thought to impede P_i's exit are weak electrostatic interactions. Therefore, a model in which the powerstroke occurs while P_i remains in the active site, and thus precedes P_i release, seems the most plausible explanation for these findings (Figure 4).

Our findings also suggest that myosin transiently exists in a post-powerstroke state while P_i remains bound in the active site; a structure that has yet to be captured using x-ray crystallography (Geeves & Holmes, 2005; Llinas et al., 2015; Rayment et al., 1993b; Smith & Rayment, 1996). The reasons for this are unclear, however there are several plausible explanations why this structural state might be difficult to capture; first among these is the inability to crystallize myosin in the presence of actin filaments. This structure is thought to be occupied only while myosin is strongly bound to the actin filament (Geeves & Holmes, 2005; Takagi et al., 2004; Woody et al., 2019), thus it may be extremely difficult to reproduce such a structure without an actin filament. While recent advances in cryo-electron microscopy may present an alternative method to obtain this structure, the speed of both the powerstroke $\geq 500 \cdot s^{-1}$ (Figure 2e) and P_i-release ($150–200 \cdot s^{-1}$ [Forgacs et al., 2009; Llinas et al., 2015; Trivedi et al., 2015]) suggest the state is very transient and therefore will be difficult to capture by this methodology. This is supported by the observation that a prepowerstroke-like state can only be captured when myosin is trapped in a transition-like state using ADP and either beryllium, vanadate or aluminum fluoride (Dominguez, Freyzon, Trybus, & Cohen, 1998; Mentes et al., 2018; Reubold, Eschenburg, Becker, Kull, & Manstein, 2003; Smith & Rayment, 1996). It is also clear from single muscle fiber experiments (Debold et al., 2004; Hibberd et al., 1985) and more recently from single molecule studies using an ultra-fast load-clamp laser trap assay (Woody et al., 2019), that myosin's affinity for P_i is strain-dependent, with P_i more readily rebinding to the active site under a high force opposing the direction of the powerstroke, a conclusion also reached based on experiments using myosin Va in a load-clamped laser trap (Sellers & Veigel, 2010). Such a strain would not be present under the conditions currently employed to obtain either x-ray crystallography or cryo-EM structures of myosin.

Our findings are, however, consistent with reports on myosin's structural dynamics in solution using FRET probes, where lever arm rotation is observed to occur very rapidly ($300–450 \cdot s^{-1}$) and is a least two-fold faster than the release of P_i into solution (Muretta et al., 2015; Trivedi et al., 2015). Our findings are also consistent with FRET studies demonstrating that, upon strongly binding to actin, the cleft in the actin-binding domain rapidly closes and that this closure is coupled to rotation of the lever arm from the pre- to postpowerstroke state (Conibear et al., 2003; Yengo et al., 2002). And it appears that the closure of the actin-binding cleft occurs prior to the release of P_i, based on a combination of FRET and kinetic experiments (Sun et al., 2008). This is also supported by recent x-ray crystallography

structures showing that myosin exhibits a closed cleft during the weak- to strongly bound transition with ADP and P_i still in the active site (Franz et al., 2020). Taken together with the present observations, these findings suggest that formation of the strong-bond with actin is the structural event that triggers the powerstroke rather than the release of P_i from the active site.

3.2 | The myosin Va powerstroke occurs in two phases

Myosin Va has been shown to have two lever arm rotations: a large (60–70°) rotation, called the primary powerstroke, which occurs upon the formation of strong-binding to actin; and a smaller rotation (10°), or hitch, thought to gate ADP-release (Sellers & Veigel, 2010; Trivedi et al., 2015). These two phases of the powerstroke are also seen in FRET assays where the rotation of the lever arm is monitored in solution (Trivedi et al., 2015). The first powerstroke occurs at a rate of $\sim 400 \cdot s^{-1}$ and in these FRET-based studies occurs faster, and prior to, the release of P_i ($150–200 \cdot s^{-1}$) in myosin Va (Trivedi et al., 2015). The secondary powerstroke occurs much more slowly at roughly $20 \cdot s^{-1}$ (Trivedi et al., 2015) and possibly prior to ADP-release (Dominguez et al., 1998; Wells et al., 1999). Ensemble averaging analysis in the present study confirms that we observed this secondary powerstroke (hitch) in our 1IQ construct (Figure 2a). The displacement generated by this hitch was ~25% of the total displacement of the powerstroke, which is consistent with previous observations in myosin Va (Sellers & Veigel, 2010; Veigel et al., 2005). The magnitude of this secondary powerstroke was unaffected by P_i in the WT construct suggesting that it is completed prior to the release of ADP, as has been suggested previously (Gunther et al., 2020). However, with only the longest 25% of the events affected by P_i (Figure 3a,c) it is possible that the rebinding of P_i does indeed prevent the secondary powerstroke but occurred in too few events to significantly decrease the size of the hitch in the ensemble average.

3.3 | P_i can rebind to myosin's active site under minimal strain

It is a widely held view that P_i does not readily rebind to myosin in the absence of a significant resistive load or strain (Geeves & Holmes, 2005; Sweeney & Houdusse, 2010; Takagi et al., 2004). However, the present findings demonstrate that in a single molecule laser trap assay, in which myosin experiences very low loads (~0.28 pN), elevated levels of P_i altered the distribution of event lifetimes (Figure 3b). At the ATP concentration used (100 μM), this provides evidence that P_i rebound to the active site in an AM.ADP state, and induced detachment from actin an AM.ADP. P_i state. Prior experiments using a laser trap assay capable of applying load to an attached cross-bridge suggested that P_i may only rebind to a strained cross-bridge using either myosin Va (Sellers & Veigel, 2010) or cardiac myosin (Woody et al., 2019), however lower concentrations of P_i (10 mM)

were used in these investigations, therefore we may have observed rebinding at lower loads due to the higher concentration of P_i levels (30 mM) increasing the probability of rebinding. Furthermore, our data suggest that only the longest lasting attachments were eliminated in the presence of elevated P_i (Figure 3a), therefore the combination of a high $[P_i]$ and long-lived AM.ADP state may be required to elicit rebinding under minimal resistive strain. Such an effect would be expected to reduce drag on actin filaments under unloaded conditions, as P_i rebinding detaches the longest lived strongly bound cross-bridges. Consistent with this idea, elevated P_i levels increase actin filament velocity in an in vitro assay (Debold et al., 2011), and unloaded shortening velocity in skinned single muscle fibers (Pate & Cooke, 1989). P_i-induced acceleration of detachment also appears to occur in myosin Va, where elevated levels of P_i shorten myosin Va's run length on an actin filament in an unloaded, single molecule, TIRF assay (Baker et al., 2004).

3.4 | What is the fate of the cross-bridge after P_i rebinds?

When phosphate rebinds to myosin II's active site in an AM.ADP state it accelerates detachment from actin (Baker et al., 2002; Debold et al., 2013; Takagi et al., 2004). The P_i-induced decrease in event lifetime observed in the present study (Figure 3a) confirms that this also occurs in myosin Va, but what is the fate of the cross-bridge after P_i rebinds to the active site? If the powerstroke can only occur after P_i-release from the active site, then it would be expected that the rebinding of P_i would prevent the powerstroke from occurring and then accelerate detachment from actin, as suggested based on structural observations (Llinas et al., 2015; Robert-Paganin et al., 2020; Sweeney & Houdusse, 2010). However, our observation that the powerstroke occurs rapidly upon binding to actin (Figures 1 and 2) is inconsistent with the powerstroke occurring after P_i-release. Our results suggest that myosin's detachment prior to the generation of the powerstroke is not the fate of a cross-bridge following the rebinding of P_i to the active site.

In contrast, if the powerstroke precedes P_i-release from the active site, the powerstroke may be reversed once P_i rebinds to the active site, returning the cross-bridge to the prepowerstroke AM.ADP. P_i state from which detachment occurs rapidly (Dantzig et al., 1992; Takagi et al., 2004). Indeed, in single molecule laser trap assays, displacements in the opposite direction of the original powerstroke have been observed, in particular under a high resistive load, and may occur more readily in the presence of P_i (Takagi et al., 2004; Woody et al., 2019). However, the position of the lever arm was not directly monitored in these prior studies so it is not clear if the backward motion detected was a reverse of the lever arm rotation or if the high resistive load caused myosin to slip on actin (Debold et al., 2005). These observations were further complicated by the use of low ATP concentrations (1 μM), which increases the probability that P_i rebound not to an AM.ADP state but the rigor state, creating an AM. P_i state instead of an AM,ADP.P_i state (Amrute-Nayak et al., 2008).

In the present study we did not see evidence of a reversal of myosin's powerstroke in the presence of elevated P_i, under any condition or using either construct (Figures 1a and 2a). If present, reversals should have been evident as an abrupt reversal of the displacement following a powerstroke while in a low variance state, but this was not seen in the raw displacement records (Figure 1a). Even if such reversals occurred with low frequency, they should have been evident as a downward slope at the back end of binding events in ensemble averaging, but again this was not observed for either construct or in the presence of P_i (Figure 2a). It is possible that such reversals occurred faster than the time resolution of our instrument (~2 ms) and therefore were invisible in the present study. If this was the case it would put time constraints on the rate of the reversal and the duration of the AM.ADP.P_i state following a reversal, indeed both events would have to occur at $>500 \cdot s^{-1}$ to have been invisible in our analyses. A recent report, using cardiac myosin II, suggested that reversals occur as slow as $250 \cdot s^{-1}$ (Woody et al., 2019), thus it would have to occur more quickly in myosin Va for it to be invisible in the present investigation.

Alternatively, it is possible that myosin detaches from actin without reversing the powerstroke following P_i-rebinding, as has been proposed (Debold et al., 2013). In this type of model, the rebinding of P_i induces detachment from a postpowerstroke state by introducing a P_i-dependent branch in the cross-bridge pathway (blue arrows, Figure 4). This kind of model can also explain the P_i-induced reduction in muscle force and offers an explanation for two observations that have been difficult to reconcile with a model containing a reversal of the powerstroke (Debold et al., 2013). Specifically, the P_i-induced enhancement of actin filament velocity at low pH in the motility assay (Debold et al., 2011; Greenberg & Moore, 2010) and the maintenance of a high ATPase rate when P_i levels are elevated despite large reductions in isometric force of muscle (Linari et al., 2010). Indeed, in the present study elevated levels of P_i had little or no effect on actin filament velocity in a motility assay using either the WT or S217A construct (Figure 3d). If P_i induced reversals of the powerstroke while myosin was strongly bound to actin, we would have expected to see a decrease in V_{actin}. Thus, a model of the cross-bridge cycle in which the rebinding of P_i can induce detachment from a postpowerstroke state is the most plausible and provides the best explanation of functional and structural findings (Figure 4).

4 | CONCLUSIONS

We used two independent approaches to maintain P_i in myosin Va's active site while directly observing its ability to bind to actin and generate a powerstroke. In both cases myosin generated a powerstroke rapidly upon binding to actin, providing strong evidence that myosin generates its powerstroke when P_i is still in its active site. This is consistent with a model in which the formation of the strongly bound state drives rotation of the lever arm and that this key force-generating event occurs before the release of P_i from the active site (Muretta et al., 2015; Takagi et al., 2004; Trivedi et al., 2015). Thus,

these findings provide crucial new insight into the molecular mechanism of force generation by myosin, and how it is coupled with the release of the gamma-P_i from myosin, and in doing so reveals new insight into how myosin transduces chemical energy into mechanical work.

5 | METHODS

5.1 | Protein construction, expression, and purification

The single-headed myosin Va S1 constructs used were constructed as previously described (Gunther et al., 2020) based on a chicken myosin Va sequence, containing the first IQ domain (residues 1–792), N-terminal tetracysteine motif, and C-terminal Myc and FLAG tags. The S217A substitution was introduced using Quikchange site directed mutagenesis (Stratagene) and co-expressed with calmodulin in baculovirus. Expressed proteins were purified using FLAG affinity chromatography. The purified proteins were then mixed with 5% sucrose and rapidly frozen using liquid notrogen in 20 μl aliquots, and thawed on the day of an experiment. The data reported were collected from five different protein preparations. Actin filaments were isolated from chicken skeletal muscle using methods previously described. For laser trapping assays, isolated actin filaments were labeled with phalloidin/TRITC and phalloidin/biotin in a 50/50 mixture. For motility experiments actin filaments were only labeled with TRITC.

5.2 | Single molecule laser trap assay

The size of myosin's powerstroke and the duration of strong-binding to the actin filament were directly determined using a three-bead laser trap assay as previously detailed (Longyear et al., 2017). Briefly, myosin was adhered to a nitrocellulose-coated coverslip under which 3 μm silica microspheres served as pedestals for the myosin. Myosin was added at a concentration of 0.7 μg/ml to a flowcell precoated with anti-myC antibody (0.8 μg/ml, Sigma Inc.) as a substrate for the myosin S1 constructs. Following the addition of myosin, BSA was an incubated in the flow cell for 5 min to inhibit nonspecific interactions between the actin filament and the coverslip surface. To initiate an experiment, a buffer including streptavidin-coated 1 μm silica microspheres (Bangs Labs Inc.), biotin/TRITC-labeled actin, oxygen scavenger system (29 mM of glucose, 1.5 mM glucose oxidase, and 80 units catalase), 91 mM KCl, 1 mM EGTA, 4 mM $MgCl_2$, and 1 mM DTT at pH 7.0, 25°C and at an ATP concentration of 100 μM. For experiments involving 30 mM added P_i, the concentration of KCl was reduced to maintain the total ionic strength of 125 mM, calculated using the Debye–Huekel Equation.

A three-axis piezo-controlled stage (Mad City Labs, Inc.) was manipulated to attach a TRITC/biotin-labeled actin filament to two 1 μm neutravidin-coated silica microspheres (Bangs Labs Inc.) held in two time-shared laser traps. Once attached to the 1 μm microspheres, the filament was extended between the optically trapped microspheres, placing 3–4 pN of pretension on the filament. At the laser power used, the two-trap stiffness of the bead-actin-bead assembly was 0.04pN/nm, as determined using the equipartition method (Dupuis et al., 1997). The bead-actin-bead assembly was then brought into close proximity to the 3 μm myosin-coated silica pedestal beads (Bangs Labs Inc.) with bead-actin-bead assembly. Single molecule activity was observed at <1 in 10 of the 3 μm pedestals interrogated, ensuring a single molecule regime. Once actomyosin binding activity was established the position of the trapped bead was recorded from the output of the quadrant photodiode, at sampling rate of 5 kHz.

5.3 | Single molecule laser assay data analysis

Laser trap data were analyzed using custom programs in R (v4.0.4, R Core Team). A two-state Hidden–Markov Model (Smith et al., 2001; Visser & Speekenbrink, 2010) was used to identify binding events from running mean and variance transformations of the laser trap data. The windows used to calculate the mean and variance had a width of 150 datapoints and progressed with half overlap. Estimations of the start and end of each binding event can be inferred in the original raw data from the results of the Hidden–Markov Model by multiplying the first and last running window position (or indexed position) that comprises an attachment event by the sliding window width (75 data points). A changepoint analysis (Killick & Eckley, 2014) was then applied to a small subset of data surrounding these transition locations (2 window widths on either side of the start and end of each binding event). The changepoint analysis was performed using the running variance of the displacement data (a 50 data point window progressing one data point at a time). The results of the changepoint analysis identified the most probable datapoint of the transition into, or out of, a binding event. Using the running variance to determine the start of the binding events allowed the changepoint analysis the ability to capture events that bound (decreasing signal variance) without producing a powerstroke. In contrast, the algorithm for detecting the end of binding events used a changepoint analysis that incorporated both the change in mean and variance of the signal as previously described (Blackwell et al., 2021). The magnitude of single molecule displacements (i.e., size of the powerstroke) were calculated by averaging the position between the start/end of each event (excluding the first and last 5 ms) and then subtracting that value from the average position preceding the transition into each event. The binding event lifetimes were determined as the duration of time between the start and end of each event, as identified by the changepoint analysis.

Ensemble averaging was performed by aligning the start and end of each event, synchronizing events by extending all events to the same duration, averaging the resulting positional data, and fitting the forward ensembles with a double exponential ($y = d_1 *(1-\exp[x^* - k_0]) + d_2 *(1 - \exp[x^* - k_1])$) and the backwards with a single exponential ($y = d_1 + d_2 *\exp[x^* k_2]$). In these equations d_1 putatively represents the displacement caused by the primary powerstroke, d_2

the displacement of the secondary powerstroke and k_2 the rate of exiting the binding event (Capitanio et al., 2006; Veigel et al., 2003).

5.4 | Simulations of single molecule binding events

These simulations were performed using *R* (v4.0.4, R Core Team). Two datasets were simulated using a kinetic scheme for S217A (Figure 4). In the first simulation, the powerstroke occurred before the P_i-release from the active and in the second series of simulations P_i-release preceded the powerstroke. The rate of P_i-release used in the simulation was $30 \cdot s^{-1}$, roughly corresponding to the average experimentally measured rates in solution ($16 \cdot s^{-1}$, $41 \cdot s^{-1}$, and $27 \cdot s^{-1}$; Forgacs et al., 2009; Gunther et al., 2020; Llinas et al., 2015). Complete details of these simulations are provided in Figure S1.

In vitro motility data. In vitro motility experiments were performed using equipment previously described (Debold et al., 2011). Preparation began with anti-myC antibody being introduced into a nitrocellulose-coated coverslip surface at a saturating concentration of 50 μg/ml and incubated for 2 min before the myosin Va construct was added at 100 μg/ml in a high-salt myosin buffer (300 mM KCl, 25 mM imidazole, 1 mM EGTA, 4 mM MgCl$_2$, 1 mM dithiothreitol). BSA was then added at 0.5 mg/ml and allowed to incubate for 5 min. 100% TRITC-labeled actin was then added in the absence of ATP before the final experimental buffer (2 mM ATP, 91 mM KCl, 1 mM EGTA, 4 mM MgCl$_2$, and 1 mM DTT at pH 7.0) was added, containing either 0.5% methylcellulose with an oxygen scavenging system as indicated above. For the experiments using 30 mM P_i the KCl was decreased in the experimental buffer to maintain a constant total ionic strength of 125 mM and the temperature maintained at 30.0°C for all experiments. During each experiment three, 30 s video recordings were made at 10 frames$\cdot s^{-1}$ at three different locations within each flow cell. A two-way ANOVA (Myosin construct $\times$ P_i level) was used to determine significant ($p < .05$) differences.

AUTHOR CONTRIBUTIONS
Edward P. Debold conceptualized the study; Brent Scott, Christopher Marang, and Edward P. Debold performed experiments, analyzed data, and wrote paper; Edward P. Debold, Christopher Marang, and Brent Scott analyzed data; Brent Scott and Mike Woodward generated figures.

DATA AVAILABILITY STATEMENT
The raw and analyzed data will be made available upon request and will be posted to an open access data sharing site.

REFERENCES

Amrute-Nayak, M., Antognozzi, M., Scholz, T., Kojima, H., & Brenner, B. (2008). Inorganic phosphate binds to the empty nucleotide binding pocket of conventional myosin II. *Journal of Biological Chemistry*, *283*(7), 3773–3781. https://doi.org/10.1074/jbc.M706779200

Bagshaw, C. R., & Trentham, D. R. (1974). The characterization of myosin-product complexes and of product-release steps during the magnesium ion-dependent adenosine triphosphatase reaction. *The Biochemical Journal*, *141*(2), 331–349. https://doi.org/10.1042/bj1410331

Baker, J. E., Brosseau, C., Joel, P. B., & Warshaw, D. M. (2002). The biochemical kinetics underlying Actin movement generated by one and many skeletal muscle myosin molecules. *Biophysical Journal*, *82*(4), 2134–2147. https://doi.org/10.1016/S0006-3495(02)75560-4

Baker, J. E., Krementsova, E. B., Kennedy, G. G., Armstrong, A., Trybus, K. M., & Warshaw, D. M. (2004). Myosin V processivity: Multiple kinetic pathways for head-to-head coordination. *Proceedings of the National Academy of Sciences of the United States of America*, *101*(15), 5542–5546. https://doi.org/10.1073/pnas.0307247101

Blackwell, T., Stump, W. T., Clippinger, S. R., & Greenberg, M. J. (2021). Computational tool for ensemble averaging of single-molecule data. *Biophysical Journal*, *120*(1), 10–20. https://doi.org/10.1016/j.bpj.2020.10.047

Capitanio, M., Canepari, M., Cacciafesta, P., Lombardi, V., Cicchi, R., Maffei, M., … Bottinelli, R. (2006). Two independent mechanical events in the interaction cycle of skeletal muscle myosin with Actin. *Proceedings of the National Academy of Sciences of the United States of America*, *103*(1), 87–92. https://doi.org/10.1073/pnas.0506830102

Capitanio, M., Canepari, M., Maffei, M., Beneventi, D., Monico, C., Vanzi, F., … Pavone, F. S. (2012). Ultrafast force-clamp spectroscopy of single molecules reveals load dependence of myosin working stroke. *Nature Methods*, *9*(10), 1013–1019. https://doi.org/10.1038/nmeth.2152

Conibear, P. B., Bagshaw, C. R., Fajer, P. G., Kovács, M., & Málnási-Csizmadia, A. (2003). Myosin cleft movement and its coupling to actomyosin dissociation. *Nature Structural Biology*, *10*(10), 831–835. https://doi.org/10.1038/nsb986

Coureux, P.-D., Sweeney, H. L., & Houdusse, A. (2004). Three myosin V structures delineate essential features of chemo-mechanical transduction. *The EMBO Journal*, *23*(23), 4527–4537. https://doi.org/10.1038/sj.emboj.7600458

Cruz, E. M. D. L., Wells, A. L., Rosenfeld, S. S., Ostap, E. M., & Sweeney, H. L. (1999). The kinetic mechanism of myosin V. *Proceedings of the National Academy of Sciences of the United States of America*, *96*(24), 13726–13731. https://doi.org/10.1073/pnas.96.24.13726

Dantzig, J. A., Goldman, Y. E., Millar, N. C., Lacktis, J., & Homsher, E. (1992). Reversal of the cross-bridge force-generating transition by photogeneration of phosphate in rabbit psoas muscle fibres. *The Journal of Physiology*, *451*, 247–278. https://doi.org/10.1113/jphysiol.1992.sp019163

Debold, E. P., Dave, H., & Fitts, R. H. (2004). Fiber type and temperature dependence of inorganic phosphate: Implications for fatigue. *American Journal of Physiology-Cell Physiology*, *287*(3), C673–C681. https://doi.org/10.1152/ajpcell.00044.2004

Debold, E. P., Patlak, J. B., & Warshaw, D. M. (2005). Slip sliding away: Load-dependence of velocity generated by skeletal muscle myosin molecules in the laser trap. *Biophysical Journal*, *89*(5), L34–L36. https://doi.org/10.1529/biophysj.105.072967

Debold, E. P., Turner, M. A., Stout, J. C., & Walcott, S. (2011). Phosphate enhances myosin-powered Actin filament velocity under acidic conditions in a motility assay. *American Journal of Physiology-Regulatory, Integrative and Comparative Physiology*, *300*(6), R1401–R1408. https://doi.org/10.1152/ajpregu.00772.2010

Debold, E. P., Walcott, S., Woodward, M., & Turner, M. A. (2013). Direct observation of phosphate inhibiting the force-generating capacity of a

miniensemble of myosin molecules. *Biophysical Journal*, *105*(10), 2374–2384. https://doi.org/10.1016/j.bpj.2013.09.046

Dominguez, R., Freyzon, Y., Trybus, K. M., & Cohen, C. (1998). Crystal structure of a vertebrate smooth muscle myosin motor domain and its complex with the essential light chain: Visualization of the pre-power stroke state. *Cell*, *94*(5), 559–571. https://doi.org/10.1016/S0092-8674(00)81598-6

Dupuis, D. E., Guilford, W. H., Wu, J., & Warshaw, D. M. (1997). Actin filament mechanics in the laser trap. *Journal of Muscle Research and Cell Motility*, *18*(1), 17–30. https://doi.org/10.1023/a:1018672631256

Finer, J. T., Simmons, R. M., & Spudich, J. A. (1994). Single myosin molecule mechanics: Piconewton forces and nanometre steps. *Nature*, *368* (6467), 113–119. https://doi.org/10.1038/368113a0

Forgacs, E., Sakamoto, T., Cartwright, S., Belknap, B., Kovács, M., Tóth, J., ... White, H. D. (2009). Switch 1 mutation S217A converts myosin V into a low duty ratio motor. *Journal of Biological Chemistry*, *284*(4), 2138–2149. https://doi.org/10.1074/jbc.M805530200

Foth, B. J., Goedecke, M. C., & Soldati, D. (2006). New insights into myosin evolution and classification. *Proceedings of the National Academy of Sciences of the United States of America*, *103*(10), 3681–3686. https://doi.org/10.1073/pnas.0506307103

Franz, P., Ewert, W., Preller, M., & Tsiavaliaris, G. (2020). Unraveling a force-generating allosteric pathway of actomyosin communication associated with ADP and Pi release. *International Journal of Molecular Sciences*, *22*(1). https://doi.org/10.3390/ijms22010104

Geeves, M. A., & Holmes, K. C. (1999). Structural mechanism of muscle contraction. *Annual Review of Biochemistry*, *68*, 687–728. https://doi.org/10.1146/annurev.biochem.68.1.687

Geeves, M. A., & Holmes, K. C. (2005). The molecular mechanism of muscle contraction. In *Advances in protein chemistry* (Vol. 71, pp. 161–193). Elsevier. https://doi.org/10.1016/S0065-3233(04)71005-0

Greenberg, M. J., & Moore, J. R. (2010). The molecular basis of frictional loads in the in vitro motility assay with applications to the study of the loaded mechanochemistry of molecular motors. *Cytoskeleton*, *67*(5), 273–285. https://doi.org/10.1002/cm.20441

Gulick, A. M., Bauer, C. B., Thoden, J. B., Pate, E., Yount, R. G., & Rayment, I. (2000). X-ray structures of the *Dictyostelium discoideum* myosin motor domain with six non-nucleotide analogs. *The Journal of Biological Chemistry*, *275*(1), 398–408. https://doi.org/10.1074/jbc.275.1.398

Gunther, L. K., Rohde, J. A., Tang, W., Cirilo, J. A., Marang, C. P., Scott, B. D., ... Yengo, C. M. (2020). FRET and optical trapping reveal mechanisms of actin activation of the power stroke and phosphate release in myosin V. *Journal of Biological Chemistry*, *295*(51), 17383–17397. https://doi.org/10.1074/jbc.RA120.015632

Gunther, L. K., Rohde, J. A., Tang, W., Walton, S. D., Unrath, W. C., Trivedi, D. V., ... Yengo, C. M. (2019). Converter domain mutations in myosin alter structural kinetics and motor function. *Journal of Biological Chemistry*, *294*(5), 1554–1567. https://doi.org/10.1074/jbc.RA118.006128

He, Z. H., Chillingworth, R. K., Brune, M., Corrie, J. E., Trentham, D. R., Webb, M. R., & Ferenczi, M. A. (1997). ATPase kinetics on activation of rabbit and frog permeabilized isometric muscle fibres: A real time phosphate assay. *The Journal of Physiology*, *501*(Pt 1), 125–148. https://doi.org/10.1111/j.1469-7793.1997.125bo.x

Hibberd, M. G., Dantzig, J. A., Trentham, D. R., & Goldman, Y. E. (1985). Phosphate release and force generation in skeletal muscle fibers. *Science (New York, N.Y.)*, *228*(4705), 1317–1319. https://doi.org/10.1126/science.3159090

Holmes, K. C., & Geeves, M. A. (2000). The structural basis of muscle contraction. *Philosophical Transactions of the Royal Society B: Biological Sciences*, *355*(1396), 419–431.

Houdusse, A., & Sweeney, H. L. (2016). How myosin generates force on Actin filaments. *Trends in Biochemical Sciences*. *41*(12), 989–997. https://doi.org/10.1016/j.tibs.2016.09.006

Huxley, A. F., & Simmons, R. M. (1971). Proposed mechanism of force generation in striated muscle. *Nature*, *233*(5321), 533–538. https://doi.org/10.1038/233533a0

Killick, R., & Eckley, I. (2014). Changepoint: An R package for changepoint analysis. *Journal of Statistical Software*, *58*(3), 1–19.

Linari, M., Brunello, E., Reconditi, M., Fusi, L., Caremani, M., Narayanan, T., ... Irving, M. (2015). Force generation by skeletal muscle is controlled by mechanosensing in myosin filaments. *Nature*, *528*(7581), 276–279. https://doi.org/10.1038/nature15727

Linari, M., Caremani, M., & Lombardi, V. (2010). A kinetic model that explains the effect of inorganic phosphate on the mechanics and energetics of isometric contraction of fast skeletal muscle. *Proceedings of the Royal Society B: Biological Sciences*, *277*(1678), 19–27. https://doi.org/10.1098/rspb.2009.1498

Llinas, P., Isabet, T., Song, L., Ropars, V., Zong, B., Benisty, H., ... Houdusse, A. (2015). How actin initiates the motor activity of myosin. *Developmental Cell*, *33*(4), 401–412. https://doi.org/10.1016/j.devcel.2015.03.025

Longyear, T., Walcott, S., & Debold, E. P. (2017). The molecular basis of thin filament activation: From single molecule to muscle. *Scientific Reports*, *7*(1), 1822. https://doi.org/10.1038/s41598-017-01604-8

Malik, F. I., Hartman, J. J., Elias, K. A., Morgan, B. P., Rodriguez, H., Brejc, K., ... Morgans, D. J. (2011). Cardiac myosin activation: A potential therapeutic approach for systolic heart failure. *Science (New York, N.Y.)*, *331*(6023), 1439–1443. https://doi.org/10.1126/science.1200113

Mentes, A., Huehn, A., Liu, X., Zwolak, A., Dominguez, R., Shuman, H., ... Sindelar, C. V. (2018). High-resolution cryo-EM structures of Actin-bound myosin states reveal the mechanism of myosin force sensing. *Proceedings of the National Academy of Sciences of the United States of America*, *115*(6), 1292–1297. https://doi.org/10.1073/pnas.1718316115

Muretta, J. M., Rohde, J. A., Johnsrud, D. O., Cornea, S., & Thomas, D. D. (2015). Direct real-time detection of the structural and biochemical events in the myosin power stroke. *Proceedings of the National Academy of Sciences of the United States of America*, *112*(46), 14272–14277. https://doi.org/10.1073/pnas.1514859112

Neuman, K. C., & Block, S. M. (2004). Optical trapping. *Review of Scientific Instruments*, *75*(9), 2787–2809. https://doi.org/10.1063/1.1785844

Pate, E., & Cooke, R. (1989). Addition of phosphate to active muscle fibers probes actomyosin states within the powerstroke. *Pflugers Archiv: European Journal of Physiology*, *414*(1), 73–81. https://doi.org/10.1007/bf00585629

Piazzesi, G., Reconditi, M., Linari, M., Lucii, L., Sun, Y.-B., Narayanan, T., ... Irving, M. (2002). Mechanism of force generation by myosin heads in skeletal muscle. *Nature*, *415*(6872), 659–662. https://doi.org/10.1038/415659a

Rayment, I., Holden, H. M., Whittaker, M., Yohn, C. B., Lorenz, M., Holmes, K. C., & Milligan, R. A. (1993a). Structure of the actin-myosin complex and its implications for muscle contraction. *Science*, *261* (5117), 58–65. https://doi.org/10.1126/science.8316858

Reubold, T. F., Eschenburg, S., Becker, A., Kull, F. J., & Manstein, D. J. (2003). A structural model for actin-induced nucleotide release in myosin. *Nature Structural Biology*, *10*(10), 826–830. https://doi.org/10.1038/nsb987

Robert-Paganin, J., Pylypenko, O., Kikuti, C., Sweeney, H. L., & Houdusse, A. (2020). Force generation by myosin motors: A structural perspective. *Chemical Reviews*, *120*(1), 5–35. https://doi.org/10.1021/acs.chemrev.9b00264

Rosenfeld, S. S., & Sweeney, H. L. (2004). A model of myosin V processivity. *Journal of Biological Chemistry*, *279*(38), 40100–40111. https://doi.org/10.1074/jbc.M402583200

Sellers, J. R., & Veigel, C. (2010). Direct observation of the myosin-Va power stroke and its reversal. *Nature Structural & Molecular Biology*, *17* (5), 590–595. https://doi.org/10.1038/nsmb.1820

Shen, M., Zhang, N., Zheng, S., Zhang, W.-B., Zhang, H.-M., Lu, Z., ... Li, X. (2016). Calmodulin in complex with the first IQ motif of myosin-5a functions as an intact calcium sensor. *Proceedings of the National Academy of Sciences of the United States of America*, 113(40), E5812–E5820. https://doi.org/10.1073/pnas.1607702113

Sleep, J., Irving, M., & Burton, K. (2005). The ATP hydrolysis and phosphate release steps control the time course of force development in rabbit skeletal muscle. *The Journal of Physiology*, 563(Pt 3), 671–687. https://doi.org/10.1113/jphysiol.2004.078873

Smith, C. A., & Rayment, I. (1996). X-ray structure of the magnesium(II)·ADP·vanadate complex of the *Dictyostelium discoideum* myosin motor domain to 1.9 Å resolution. *Biochemistry*, 35(17), 5404–5417. https://doi.org/10.1021/bi952633+

Smith, D. A., Steffen, W., Simmons, R. M., & Sleep, J. (2001). Hidden-Markov methods for the analysis of single-molecule actomyosin displacement data: The variance-hidden-Markov method. *Biophysical Journal*, 81(5), 2795–2816. https://doi.org/10.1016/S0006-3495(01)75922-X

Sun, M., Rose, M. B., Ananthanarayanan, S. K., Jacobs, D. J., & Yengo, C. M. (2008). Characterization of the pre-force-generation state in the actomyosin cross-bridge cycle. *Proceedings of the National Academy of Sciences of the United States of America*, 105(25), 8631–8636. https://doi.org/10.1073/pnas.0710793105

Sweeney, H. L., & Houdusse, A. (2010). Structural and functional insights into the myosin motor mechanism. *Annual Review of Biophysics*, 39, 539–557. https://doi.org/10.1146/annurev.biophys.050708.133751

Takagi, Y., Homsher, E. E., Goldman, Y. E., & Shuman, H. (2006). Force generation in single conventional Actomyosin complexes under high dynamic load. *Biophysical Journal*, 90(4), 1295–1307. https://doi.org/10.1529/biophysj.105.068429

Takagi, Y., Shuman, H., & Goldman, Y. E. (2004). Coupling between phosphate release and force generation in muscle actomyosin. *Philosophical Transactions of the Royal Society of London Series B, Biological Sciences*, 359(1452), 1913–1920. https://doi.org/10.1098/rstb.2004.1561

Trivedi, D. V., Muretta, J. M., Swenson, A. M., Davis, J. P., Thomas, D. D., & Yengo, C. M. (2015). Direct measurements of the coordination of lever arm swing and the catalytic cycle in myosin V. *Proceedings of the National Academy of Sciences of the United States of America*, 112(47), 14593–14598. https://doi.org/10.1073/pnas.1517566112

Vale, R. D. (1996). Switches, latches, and amplifiers: Common themes of G proteins and molecular motors. *The Journal of Cell Biology*, 135(2), 291–302. https://doi.org/10.1083/jcb.135.2.291

Vale, R. D. (2003). The molecular motor toolbox for intracellular transport. *Cell*, 112(4), 467–480. https://doi.org/10.1016/S0092-8674(03)00111-9

Veigel, C., Molloy, J. E., Schmitz, S., & Kendrick-Jones, J. (2003). Load-dependent kinetics of force production by smooth muscle myosin measured with optical tweezers. *Nature Cell Biology*, 5(11), 980–986. https://doi.org/10.1038/ncb1060

Veigel, C., Schmitz, S., Wang, F., & Sellers, J. R. (2005). Load-dependent kinetics of myosin-V can explain its high processivity. *Nature Cell Biology*, 7(9), 861–869. https://doi.org/10.1038/ncb1287

Visser, I., & Speekenbrink, M. (2010). depmixS4: An R package for Hidden Markov models. *Journal of Statistical Software*, 36(1), 1–21. https://doi.org/10.18637/jss.v036.i07

Warshaw, D. M., Kennedy, G. G., Work, S. S., Krementsova, E. B., Beck, S., & Trybus, K. M. (2005). Differential labeling of myosin V heads with quantum dots allows direct visualization of hand-over-hand processivity. *Biophysical Journal*, 88(5), L30–L32. https://doi.org/10.1529/biophysj.105.061903

Wells, A. L., Lin, A. W., Chen, L.-Q., Safer, D., Cain, S. M., Hasson, T., ... Sweeney, H. L. (1999). Myosin VI is an actin-based motor that moves backwards. *Nature*, 401(6752), 505–508. https://doi.org/10.1038/46835

Woody, M. S., Winkelmann, D. A., Capitanio, M., Ostap, E. M., & Goldman, Y. E. (2019). Single molecule mechanics resolves the earliest events in force generation by cardiac myosin. *eLife*, 8, e49266. https://doi.org/10.7554/eLife.49266

Yengo, C. M., de la Cruz, E. M., Chrin, L. R., Gaffney, D. P., & Berger, C. L. (2002). Actin-induced closure of the Actin-binding cleft of smooth muscle myosin*. *Journal of Biological Chemistry*, 277(27), 24114–24119. https://doi.org/10.1074/jbc.M111253200

Yildiz, A., Forkey, J. N., McKinney, S. A., Ha, T., Goldman, Y. E., & Selvin, P. R. (2003). Myosin V walks hand-over-hand: Single fluorophore imaging with 1.5-nm localization. *Science*, 300(5628), 2061–2065. https://doi.org/10.1126/science.1084398

SUPPORTING INFORMATION

Additional supporting information may be found online in the Supporting Information section at the end of this article.